Seismic Performance Evaluation of Skew Reinforced Concrete Bridges with LRB and FPS Isolation Systems

Authors:

Mohammad Naghibi[1], Shima Mahboubi[1, *], Mahmood Reza Shiravand[1]

Abstract

Recent earthquake highlighted the vulnerability of skew bridges to seismic loads, particularly under near-fault events. In contrast, seismically isolated bridges are among the most commonly used bridges in seismic prone regions. This paper aims to investigate the effect of skew angle on seismic performance of reinforced concrete (RC) bridges isolated with two base isolation systems including the Friction Pendulum System (FPS) and Lead Rubber Bearings (LRB). For this purpose, finite element models of RC bridges with different skew angles (0°, 15°, 30°, 45°, and 60°) isolated with FPS and LRB were developed and evaluated through incremental dynamic analyses using a series of 20 near-fault ground motions records. Then, fragility curves of isolated bridge models with different skew angles were developed and compared to assess the seismic response of the isolators. The results show that larger skew angles increase the probability of damage in RC bridge piers, particularly at higher damage levels. Furthermore, skew bridges isolated with FPS consistently exhibit greater seismic stability than those with LRB across all skew angles. These results advance the understanding of the seismic fragility of base-isolated skew bridges and provide practical guidance for performance-based design and retrofitting in near-fault regions.

Keywords: Skew Bridges, Lead Rubber Bearings, Friction Pendulum System, Fragility Curves, Incremental Dynamic Analysis

1. Faculty of Civil, Water and Environmental Engineering, Shahid Beheshti University, Tehran, Iran

*Corresponding Author: sh_mahboubi@sbu.ac.ir

1. Introduction

Bridges are important components of highway transportation systems that link different areas, such as rivers, valleys, highways, and other difficult terrains. The bridge role in reducing travel time, enabling trade, providing access to remote regions, and ensuring efficient service delivery is crucial for modern societies and economies (Koks et al., 2019; Smith et al., 2021). Bridges are those in which the piers and abutments are built at a skew angle. In these structures, the piers cannot be placed perpendicular to the longitudinal axis of the bridge deck, and instead are positioned with a certain skew, usually due to construction limitations such as crossing rivers, railways, or roadways (Coletti et al., 2011). A considerable portion of the global bridge inventory consists of skew bridges, making their seismic performance a critical concern for both engineers and researchers. Unlike straight bridges, skew bridges exhibit distinct seismic behavior, as their geometry induces coupled translational and torsional responses during earthquakes. This, in turn, results in uneven force distribution across structural components and complex failure mechanisms (Ateş et al., 2024). Such behavior often amplifies demands on bearings, piers, and abutments, thereby increasing the likelihood of premature damage or collapse. The problem is particularly acute for reinforced concrete (RC) bridges, where discontinuities in the superstructure further heighten vulnerability, especially under near-fault ground motions.

Extensive research has been devoted to the seismic fragility of skew bridges. Argyroudis et al. proposed a resilience-oriented framework, highlighting that geometric irregularities diminish resilience along critical transportation corridors (Argyroudis et al., 2020). Y. Dong et al. developed a probabilistic model for mainshock–aftershock sequences, demonstrating that aftershocks significantly exacerbate seismic losses (Y. Dong et al., 2015). S. Aldea et al. examined common skew highway bridges in Chile before and after the 2010 Maule earthquake, concluding that retrofits reduced, but did not eliminat, seismic vulnerabilities (Aldea et al., 2024). J. Chen et al. emphasized the adverse role of abutment pounding, particularly at higher skew angles (J. Chen et al., 2017). A. Abdel-Mohti et al. and Yin et al. reported that increasing skew angles intensify torsional effects, elevate unseating risks, and undermine the reliability of conventional fragility models such as HAZUS (Abdel-Mohti et al., 2013a; Yin et al., 2023). Further investigations have addressed ground motion directionality (Noori et al., 2019), the role of isolation devices such as lead rubber bearings (LRB) (Lee et al., 2018), torsional demands in isolated frames (Ozer et al., 2025), and vertical ground motion effects in friction pendulum systems (FPS) (G.Shid et al., 2025), collectively underscoring the multifaceted challenges posed by skew bridge configurations. Despite these contributions, critical knowledge gaps persist. Much of the existing research has concentrated on straight bridges, while the complex interplay between skew geometry, superstructure damage, and seismic isolation systems under near-fault ground motions remains insufficiently understood (Abdel-Mohti et al., 2013b). Moreover, although seismic isolation is widely recognized as an effective mitigation strategy, the comparative effectiveness of commonly used isolators, such as LRB

and FPS, on the fragility of skew RC bridges has not been systematically examined. Past events, including the 1994 Northridge earthquake, have repeatedly demonstrated the heightened susceptibility of skew bridges to intense ground shaking (Meng et al., 2000; Abdel-Mohti et al., 2013a), highlighting the need for a more comprehensive evaluation.

The objective of the present study is to provide a detailed comparative assessment of the seismic performance of skew RC bridges isolated with FPS and LRB systems when subjected to near-fault ground motions. To this end, a parametric investigation is conducted on a representative five-span concrete bridge model with skew angles of 0°, 15°, 30°, 45°, and 60°. Finite element models are developed in SAP2000 with fixed-base foundations, incorporating both FPS and LRB isolation systems. Nonlinear dynamic analyses are carried out using 20 pairs of horizontal ground motion records. Subsequently, Probabilistic Seismic Demand Models (PSDMs) are derived to support fragility assessment. The engineering demand parameters (EDPs) considered include the maximum drift ratio of a typical pier column and the ultimate displacement capacity of the isolation systems, enabling the development of component-level fragility curves. This study advances the understanding of skew bridge behavior by systematically evaluating seismic vulnerability across five skew angles (0°, 15°, 30°, 45°, and 60°) under near-fault ground motions, with particular attention to the heightened demands in highly skewed configurations. A key novelty lies in the comparative assessment of two widely adopted isolation systems, friction pendulum systems (FPS) and lead rubber bearings (LRB), through fragility analyses that incorporate multiple damage states defined by pier drift and isolator displacement capacities. This dual focus provides new insights into the relative effectiveness of FPS and LRB in mitigating seismic risks for skewe RC bridges.

2. Lead Rubber Bearings

Lead Rubber Bearings (LRBs) are among the most commonly used base isolation devices in seismic design. They are efficient when it comes to earthquake-induced structural damage mitigation. Their major benefits include base shear reduction, displacement demand control, and increasing safety margins for critical facilities (P. Chen et al., 2025). Because of their nonlinear hysteretic characteristics, LRBs are extremely effective in seismic energy dissipation under moderate ground motions. But their performance can be compromised under near-fault excitations, where velocity pulses have the tendency to generate excessive displacements that exceed design limits, particularly for irregularly shaped or skew bridge configurations (Son et al., 2025). LRB design is the incorporation of mechanical and material properties with the objective of ensuring dependable performance for expected seismic loads. Some of the key design parameters include vertical load-carrying capacity, horizontal stiffness, post-yield stiffness, lead-core yield force, and maximum allowable displacement. The vertical stiffness, which is mostly regulated by the rubber layers, is adequate to withstand axial loads with no more than moderate compression. The horizontal stiffness, however, regulates the isolation period and the energy dissipation capability. The yield strength of the lead core is chosen to

realize the desired level of hysteretic damping, typically in the range of 15% to 30% of critical damping. Current codes, i.e., FHWA-NHI-15-004 (FHWA-NHI-15-004, 2014; Y.Bouassida et al., 2012), give step-by-step procedures for estimating displacement demands, capacity checking, and design checks for combined axial, shear, and torsional loading. A generic model of an LRB-type base isolation system is shown in Figure 1.
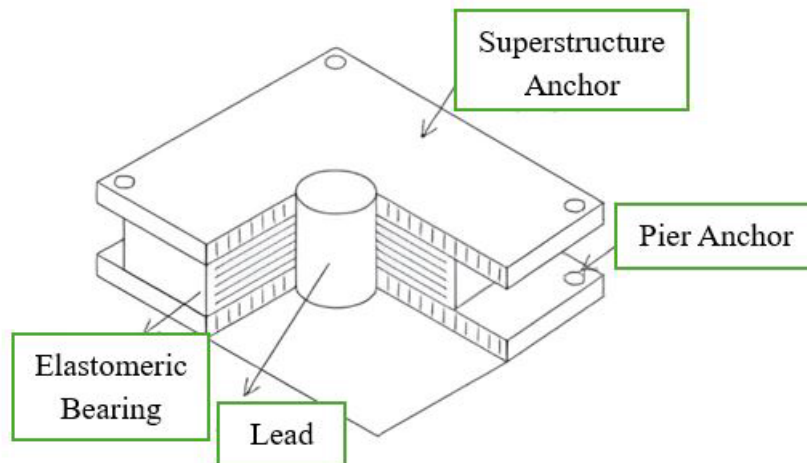

Figure 1. LRB isolation system

The main design parameters that control the LRB response are the yield force, F_y, isolator diameter D, lead-core diameter d, rubber layer quantity n, and thickness t of the layers. All of them jointly determine the mechanical behavior controlling both the capacity for carrying loads and the capacity for energy dissipation. The nonlinear force-displacement LRB behavior is normally idealized in terms of a bilinear hysteresis model, represented in Figure 1. It is described by two stiffness parameters only: the elastic (or unloading) stiffness k_e and the post-yield (plastic) stiffness k_p (Robinson et al., 2011). The bilinear relationship very well describes the elastic–hysteretic transformation of behavior and allows a realistic description of isolator behavior under seismic excitation.

The elastic stiffness k_e is defined as the ratio of the yield strength to the yield displacement, as expressed in equation $k_e = \frac{F_y}{D_y}$, while the post-yield stiffness k_p is given by the formula:

$$k_p = \frac{G.A_r}{t_r}.f_L \qquad (1)$$

where G is the shear modulus of the rubber, A_r is the cross-sectional area of the rubber layers, t_r is the total thickness of rubber consisting of n layers, and the factor f_L is equal to 1.5. The characteristic strength Q (force intercept at zero displacement) is given by the equation:

$$Q = A_{pb}.\sigma_{ypb} \qquad (2)$$

where A_{pb} is the area of lead core, and σ_{ypb} the yield strength of the lead core (ranging between 7 and 8.5 MPa). The average or effective stiffness k_{eff} is defined as the ratio between the force F_m, occurring at a specified LRB isolator displacement Δ, and the displacement Δ:

$$k_{eff} = \frac{F_m}{\Delta} \tag{3}$$

The effective stiffness k_{eff} can also be expressed as a function of the characteristic strength Q as in the following equation:

$$k_{eff} = k_p + \frac{Q}{\Delta} \qquad (\text{when } \Delta > D_y) \tag{4}$$

where D_y is the yield displacement as shown in Fig. 1. On the other hand, when the design displacement $\Delta < D_y$, the effective stiffness $k_{eff} = k_e$. The force F_m can be defined as:

$$F_m = Q + k_p . \Delta \tag{5}$$

while the yield force F_y can be obtained from:

$$F_y = Q + K_p . D_y \tag{6}$$

The area E D of the hysteretic loop can be obtained from the equation:

$$ED = 4Q . (\Delta - \Delta(y)) \tag{7}$$

This area represents the energy dissipation at each cyclic motion of LRB isolator. Then, the effective damping ratio ζ_{eff}, which produces the same amount of damping energy dissipation as the hysteretic energy dissipated at each cyclic motion of the LRB isolator, is expressed as:

$$\xi = \frac{ED}{2\pi K_{eff}\Delta^2} \tag{8}$$

Finally, the fundamental isolation period T^{iso} is given by the equation:

$$T^{iso} = 2\pi \sqrt{\frac{M}{\Sigma K_{eff}}} \tag{9}$$

where M is the total mass on the isolation system, including the mass of the superstructure and the mass of the isolation system. The term $\Sigma K_{eff} = K_{eff}$ is the total effective stiffness of the isolation system.

3. Friction Pendulum System

The Friction Pendulum System (FPS) employs pendulum movement, geometry and gravity, and has very good strength and flexibility with installation ease compared to conventional systems. Its mass, area and geometric shape and the level of friction by the sliding interface all help in achieving isolation and restoring forces. Normally built of long-lasting, weatherable

materials, FPS has been found to respond well for conventional testing under high rates of deformation corresponding with extensive earthquake conditions. FPS also illustrate a relatively higher reduction of torsional motion that has the effect of considerable reduction of seismic loads (Zayas et al., 1990). The primary drawback of FPS relies on the necessity for the systems that are engineered to be specially designed for a particular level of intensity. Conventional systems that are engineered possess constant damping and stiffness across all hazard levels in that controlling the displacements at very high earthquakes of intensity renders them vulnerable. Therefore FPS are efficient in a narrow range of seismic values (Pranesh et al., 2000). At the same time, FPS possess another disadvantage in the form of the discrepancy between the corresponding bearing pressure and the kinetic friction coefficient (Shid et al., 2025). Normally an FPS comprises of a stainless-steel-made spherical surface, an articulating slider that runs on a Polytetrafluoroethylene (PTFE) composite-steel concave sliding surface and a housing plate (Bouassida et al., 2012). The radius (R) of the curved FPS isolator and the period of isolation of the structure is calculated ($T=2\pi \sqrt{(R/g)}$ (Naeim et al., 1999) .Force-displacement hysteresis loop of the bearing of the FPS is depicted in Figure 2 (Dicleli et al., 2002)
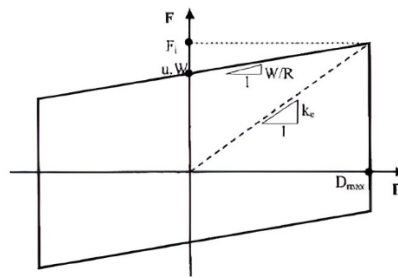

Figure 2. Force-displacement hysteresis loop for friction pendulum (Dicleli 2002)

The hysteretic behavior of friction pendulum system (FPS) is mainly influenced by three parameters: the radius of curvature of the concave surface, R; the friction coefficient, μ; and the vertical reaction force, W, acting at the bearing, where these parameters collectively determine isolation period, energy dissipation capacity, and restoring force characteristics. For bridge bearings, the effective radius, R, and the displacement demand, u, can be regarded as the pertinent design variables. The horizontal force, F transmitted at displacement, D can be described as:

$$F = \mu W \text{sgn}(\dot{\mu}) + \frac{W}{R} D \qquad\qquad (10)$$

where $\dot{\mu}$ is the sliding velocity, sgn() is the signum function (+1 or -1 depending on the motion direction). The horizontal force described previously represents the lateral resistance of the bearing, which is directly proportional to friction coefficient μ, displacement D and vertical reaction force W. For response spectrum analyses, the isolator's nonlinear behavior is often conceptualized in terms of an equivalent stiffness parameter. The equivalent bearing stiffness

Ke is defined as an equivalent stiffness, or the maximum horizontal force relative to the maximum bearing displacement Dmax, as shown in (Figure 2).

$$K_e = \frac{\mu W}{D_{max}} + \frac{W}{R} \qquad (11)$$

The FPS model depicts a bilinear relationship between the lateral force, F_L that is applied to the isolator and the resisting frictional force at the isolator interface immediately prior to sliding. The pre-sliding condition results in what is theoretically an infinite initial stiffness depicted in the hysteresis loop as the vertical line until a force is applied that is sufficient to overcome the frictional bonds. The resistance or restoring stiffness, after sliding begins, is defined for the purpose of this analysis as $K_s = {}^{mg}/_R$ Changes in the friction coefficient, μ, usually result in high variability in the seismic response, of the FPS isolators. The classical Coulomb model uses μ as a constant value, whereas experimental studies (Constantinou et al., 1999) have shown that μ varies according to the sliding velocity, and therefore can be modeled with minimum and maximum velocity demands.
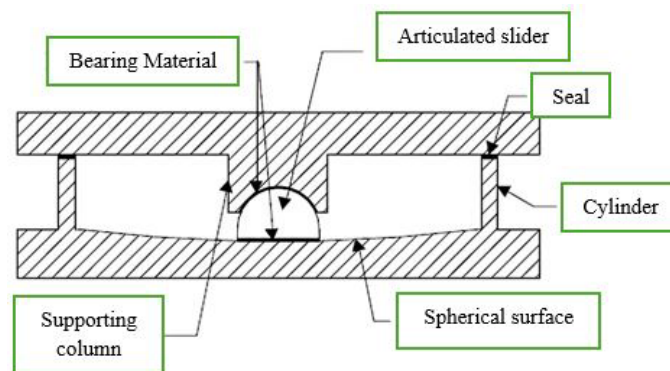

Figure 3. FPS isolation system

4. Bridge Model

The bridge selected in the present work is that of Jara et al.'s seismically isolated (Jara et al., 2016), in which Lead Rubber Bearings (LRBs) are used to act as isolators. The bridge has five spans of 30 m each in length. Five piers with a height of 15 m support each bent. Soil_structure interaction is not taken into account, and the assumption is that the piers are fixed at the foundations in all six degrees of freedom. The piers consist of a cast-in-place central reinforced concrete shaft with a diameter of 110 mm and a longitudinal reinforcement ratio of 1.5%. The bridge deck is idealized as a 0.20-m thick reinforced concrete slab with a compressive strength of 24.5 MPa and supported by prestressed concrete AASHTO type IV girders (Figure 4). Ateral connectivity of the girders in the transverse direction is supplied through diaphragms in order to enhance lateral stiffness. Diaphragms are placed at the span ends and at the one-third and

the two-third span locations. The compressive strength of the girders is taken as 34.3 MPa and that of other structural elements is taken as 24.5 MPa. Reinforcing bars are assigned a yield strength of fy=411.9 MPa. Elasticity modulus of the concrete is taken to be Ec=14000√(f$_c$). The overall width of the bridge is taken as 10.6 m with a capacity of supporting two traffic lanes. To account for additional non-structural mass and enhance superstructure weight representation more closely, the mass of the deck is increased by 25%, employing the approach formulated by Ramanathan et al (Ramanathan et al., 2012). The substructure consists of frame-type piers with four constant cross-section circular columns. The fixed-base foundations are used to model the piers and the effects of soil–structure interactions are ignored. The compressive concrete strength of the columns is given as 24.5 MPa with a center-to-center space between the adjacent columns of 1.7 m. The girders are supported on FPS and LRB isolators, located below each girder and above the bent caps. . The isolators are designed per the specific bridge characteristics and in accordance with the AASHTO Guide Specifications for Seismic Isolation Bridge Design (FHWA-NHI-15-004, 2014). The base-isolation system is in a two-line arrangement with a discontinuous deck configuration. The analytical model is set up in SAP2000 (v23.2.0, CSI 2023). Frame-type elements are utilized to model the girders, columns, diaphragms, and bent caps, and the deck and girders are taken to be elastic in seismic excitation(Ramanathan et al., 2012; Nielson et al., 2005; Nielson et al., 2007; Gkatzogias et al., 2022). A 15-mm expansion opening with a stiffness of 400 kN/m is created between neighboring decks and simulated using gap elements. The nonlinear behavior of the columns is estimated using a concentrated plasticity approach with plastic hinges distributed at the column ends near the fixity locations. The hinge properties are estimated using a moment–curvature relationship evaluated at a section at a location of 1.0 m above the column base.

Table 1. Bridge design numerical aspects

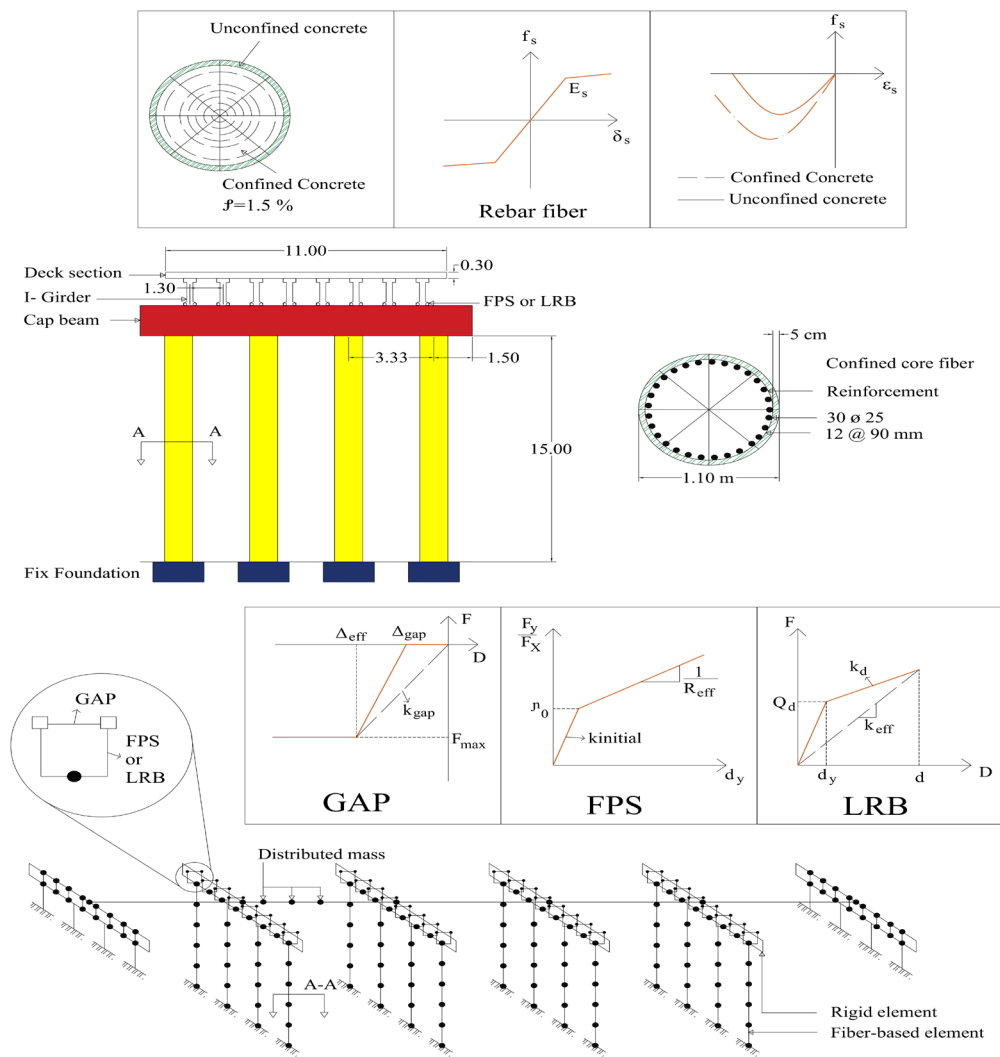| Bridge numerical aspects	Number of spans	Span length	Deck width	Girder type	Depth of girder	Number of columns per bent	Column height
	5	30 m	11 m	I-type	1.35 m	4	15 m

Figure 4. Numerical modeling of bridge components and a 3D nodal scheme of bridge model

The concrete constitutive model selected to represent the uniaxial stress-strain behavior for confined and unconfined concrete was proposed by (Mander et al., 1999), and the model used for the reinforcing steel was the one proposed by J. B. Mander (Park et al., 1975). The confined model for the core and unconfined model for concrete cover is used. According to the equation developed by Priestley et al. (Priestley et al., 1996), Eq.(1), the plastic hinge length was determined:

$$L_p = 0.08L + 0.022\ d_bf_y \geq 0.044d_bf_y \tag{12}$$

Where L_p is the hinge plastic length, L is the column length, d_b is the longitudinal bar diameter and f_y is the yield reinforcement strength. This model is used to incorporate the material nonlinearity distribution along member's lengths and cross-sections. P-Delta coordinates transformation has been employed to assume that seismic behavior could be both geometrically and materially nonlinear(Nielson et al., 2007; Padgett et al., 2008).

5. LRB and FPS Characteristics

In order to capture the nonlinear seismic behavior and reasonably predict the performance of skew bridges isolated with FPS and LRB devices, a three-dimensional nonlinear finite element model of the whole bridge was created. It considers column drift and isolator displacements and expansion joints simulated with gap elements between the discontinuous decks. These gap elements were included in order to simulate rotation effects and ponding phenomena that become prominent at larger skews. The superstructure of the bridge, with a width of 10.6 m and supported by eight girders, was simulated with gap elements at the girder centers. Nonlinear time-history analyses were performed in SAP2000 (v23.2.0, CSI 2023) with bi-direction near-field ground motions containing both pulse-like and non-pulse records

Table 2. Design parameters of the used isolators

Parameters	Unit	0-skew	15-skew	30-skew	45-skew	60-skew
		LRB	**LRB**	**LRB**	**LRB**	**LRB**
P_{dl+ll}[1]	kN	600	600	600	600	600
K_e[2]	kN/m	500	440	400	350	300
K_2[3]	kN/m	344	291.57	254.28	213.508	166.666
F_y[4]	kN	38	37	38.6	43.3	45
(K_2/K_1)[5]	-	0.18105	0.157605	0.13175	0.1331	0.1111
$\xi(\%)$[6]	-	15	18	20	22	25
D_{max}[7]	cm	20	21	23	27.5	30
Parameters						
		FPS	**FPS**	**FPS**	**FPS**	**FPS**
P_{dl+ll}	kN	600	600	600	600	600
K_e	kN/m	650	570	540	530	500
K_2	kN/m	470	406.3	396	399	380
μ[8]	-	0.06	0.06	0.06	0.06	0.06
R(recommanded)[9]	mm	2500	2500	2500	2500	2500
$\xi(\%)$	-	20	21	23	25	30
D_{max}	cm	20	22	25	27.5	30

---

[1] The summation of Dead and Live load on each isolation
[2] Effective stiffness
[3] Secondary stiffness
[4] Yield force
[5] Proportion of secondary to initial stiffness
[6] Damping ratio
[7] Maximum displacement
[8] Friction coefficient
[9] Radius of curvature surface

6. Modal Analysis

Modal analysis is a fundamental tool in structural dynamics for identifying a structure's inherent vibration characteristics, namely its natural frequencies, mode shapes, and damping properties. This approach represents the dynamic response as a superposition of independent vibration modes, each associated with a distinct natural frequency and deformation pattern. Table 3 summarizes the first three natural periods of bridge models isolated with LRB and FPS isolators across all skew angles. The results indicate that increasing skew angle leads to longer natural periods, reflecting the influence of skew geometry on dynamic flexibility. Furthermore, notable differences are observed between the natural periods of LRB- and FPS-isolated models, primarily attributable to variations in initial stiffness and yield displacement. For reference, Figure 4 presents the first three natural periods of the non-skew bridge and the corresponding mode shapes of the analyzed models.

Table 3. Periods of vibration modes of the bridge models

	Bridge Models									
Model number	**Skew angle 0°**		**Skew angle 15°**		**Skew angle 30°**		**Skew angle 45°**		**Skew angle 60°**	
Mode	FPS	LRB	FPS	LRB	FPS	LRB	FPS	LRB	FPS	LRB
First	3.135	2.674	3.1179	2.7116	3.0538	2.732	4.9265	2.94566	4.95	3.10998
Second	1.1969	1.7272	1.5032	1.7413	2.26335	1.7969	2.24861	1.8316	2.2777	1.89
Third	1.09	1.669	1.21301	1.68198	1.4	1.71134	2.173	1.77583	1.6239	1.83

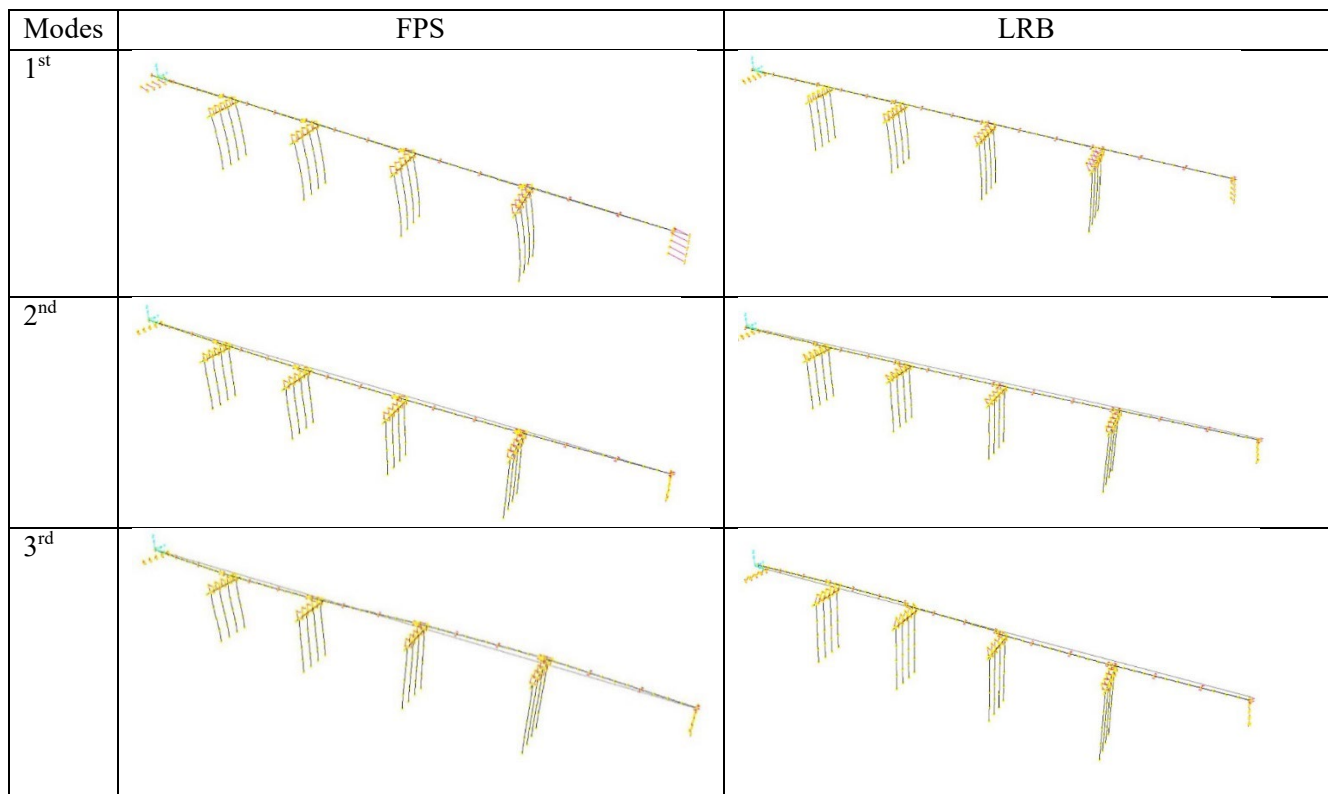| Modes	FPS	LRB
1st		
2nd		
3rd		

Figure 5. Three mode shapes based on modal analysis of non-skew bridge.

7. Selection of Ground Motions

The selection of ground motion records is a critical step in time-history analysis due to the inherent uncertainty of seismic events (Akhani et al., 2024). In this study, two categories of near-fault ground motions defined by FEMA P-695 (Applied Technology Council, 2009) are employed: records with strong velocity pulses ("NF-Pulse") and records without such pulses ("NF-No Pulse"). Both categories consist of ground motions recorded within 10 km of fault rupture. A total of 20 records (40 components) were selected from the PEER NGA database following the criteria outlined in Section A.7 of Appendix A of FEMA P-695.
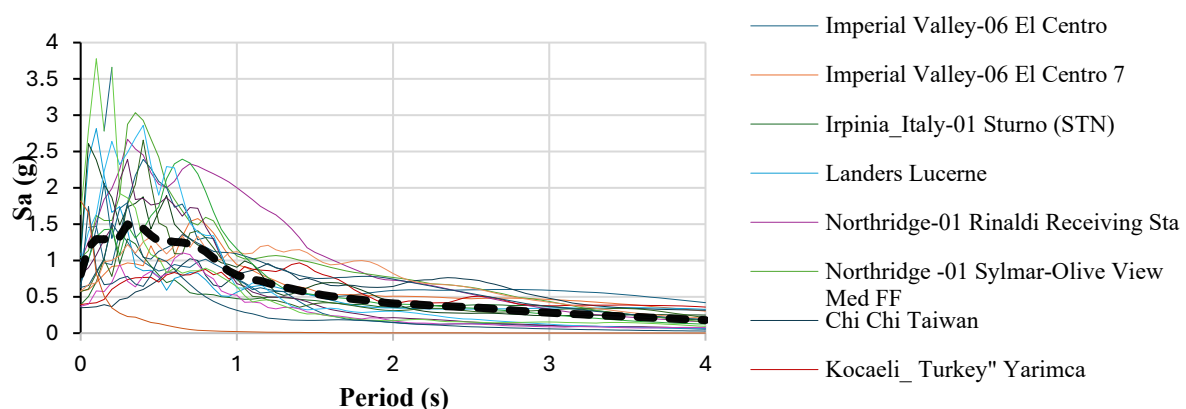

Figure 6. Acceleration response spectra of 20 ground motions

For each record, Table 4 summarizes the details such as magnitude, year and name of earthquake events and the name of the station. The twenty records are taken from 14 events that occurred between 1976 and 2002. Event magnitudes range from M6.5 to M7.5 with an average magnitude of M7.0.

Table 4. List of selected ground motion records.

No.	Earthquake	Year	Situation	Mag.(M_w)	PGA(g)
1	Imperial Valley-06	1979	El Centro Array #6	6.5	0.449
2	Imperial Valley-06	1979	El Centro Array #7	6.5	0.469
3	Superstition Hills-02	1987	Parachute Test Site	6.5	0.4318
4	Erzican_ Turkey	1992	Erzincan	6.7	0.4961
5	Cape Mendocino	1992	Petrolia	7	0.6615
6	Landers	1992	"Lucerne"	7.3	0.7887
7	Northridge-01	1994	Rinaldi Receiving Sta	6.7	0.874
8	Chi-Chi, Taiwan	1994	TCU102	6.7	0.3039
9	Duzce_ Turkey	1999	Duzce	7.6	0.5149
10	Northridge-01	1999	Sylmar - Olive View Med FF	7.1	0.8433
11	Gazli_ USSR	1976	Karakyr	6.8	0.8639
12	Imperial Valley-06	1979	Bonds Corner	6.5	0.7769
13	Imperial Valley-06	1979	Chihuahua	6.5	0.2699
14	Nahanni_ Canada	1985	Site 1	6.8	1.2
15	Nahanni_ Canada	1985	Site 2	6.8	0.5192
16	Loma Prieta	1989	BRAN	6.9	0.5022
17	"Loma Prieta	1989	Corralitos	6.9	0.5291
18	Cape Mendocino	1992	Cape Mendocino	7	1.493
19	Northridge-01	1994	LA - Sepulveda VA Hospital"	6.7	0.932
20	Kocaeli_ Turkey	1999	Yarimca	7.5	0.3218

8. Incremental Dynamic Analysis (IDA)

The Incremental Dynamic Analysis (IDA) method, introduced by Cornell et al., has become a benchmark approach for seismic performance assessment (Cornell et al., 2002). IDA establishes relationships between a seismic intensity measures (IM), such as the spectral acceleration at the fundamental period Sa (T1), and an engineering demand parameter (EDP), such as maximum column drift. This is achieved by subjecting the structure to a suite of ground motion records, each systematically scaled to increasing intensity levels, thereby capturing the full response spectrum, from initial elasticity through inelastic behavior to global or local collapse. Unlike simpler procedures such as static pushover analysis, IDA accounts for record-to-record variability, cyclic degradation, and dynamic instability, offering a comprehensive

basis for fragility assessment, collapse probability estimation, and performance-based seismic design, despite its high computational demand.

Figure 14 illustrates the IDA results for ten ground motion records, categorized by FPS- and LRB-isolated models across different skew angles. The results show that non-skewed bridges exhibit lower vulnerability, with structural failure occurring at higher PGA levels. Moreover, FPS consistently outperforms LRB, as bridges isolated with FPS demonstrate a lower probability of reaching damage states at the same PGA, indicating improved seismic resilience across all skew configurations.

(a) Skew angle of 0 with FPS base isolation

(b) Skew angle of 0 with LRB base isolation

(c) Skew angle of 30 with FPS base isolation

(d) Skew angle of 30 with LRB base isolation

(e) Skew angle of 30 with FPS base isolation

(f) Skew angle of 30 with LRB base isolation

Figure 7. IDA curves of bridges with different skew angle and isolation systems

9. Probabilistic Analyses and Fragility Curves

The fragility of a structure is characterized by the probability of reaching or exceeding predefined damage states, corresponding to a specified engineering demand parameter (EDP), conditioned on a given intensity measure (IM) as expressed in Eq. (13):

$$P[D \geq (d|IM)] = 1 - \emptyset\left(\frac{\ln d - \ln S_D}{\beta.(D|IM)}\right) \qquad (13)$$

where $\emptyset(0)$ represents the standard normal cumulative distribution function, S_D denotes the median demand conditioned on the *IM*, and $\beta(D|IM)$ is the lognormal standard deviation. For estimating the component fragility, a closed-form solution described in Eq. (14). Can be used.

$$P_f = \emptyset\left(\frac{\ln\left(S_d/S_c\right)}{\sqrt{\beta_a^2 + \beta_c^2}}\right) \qquad (14)$$

where S_D and S_C denote the median of demand and capacity and $\beta_{(D|IM)}$ and β_c denote the dispersions of demand and capacity, respectively. To define S_C and β_c, it is essential to consider the limit states listed in Table 10. For the development of fragility curves in this study, the column drift, displacement of FPSs and LRBs were selected as EDPs, and PGA was chosen as the IM.

9.1. Bridge Damage States

Several criteria for quantifying damages of bridge components have been proposed based on maximum drift, energy damping, displacement, residual drift, stiffness and etc (Dutta et al., 1998; Ashouri et al., 2024). The most frequent damage in RC bridges include pier damage, unseating of bridge spans, and bearing failure. Among these, inadequate flexural and shear strength, combined with limited ductility capacity of piers, often result in severe damage under strong ground motions. Damage indices are typically expressed in terms of structural parameters such as drift, displacement ductility, residual displacement, curvature, energy dissipation capacity, and low-cycle fatigue. Dutta et al. classified bridge column damage into four states, slight, moderate, extensive, and complete, based on drift limits, where drift is defined as the ratio of maximum column-top displacement to column height (Dutta et al., 1998). In this study, the five-level drift-based classification proposed by Dutta et al. is adopted to define the damage states, as summarized in Table 5 (Dutta et al., 1998).

Table 5. Damage states of substructure components

Bridge Component	damage threshold value				
	almost no	slight	moderate	extensive	Complete

Pier	A	Description of the physical process	First yield	Cracking and spalling	Expansion of spalling	incipient degradation	failure leading to collapse
	B	Drift (%)	0.5	0.7	1.5	2.5	5
Bearing	C	Displacement (cm)	-	-	-	-	20 - 30 cm

According to Table 5, a column drift of 0.5% indicates the onset of yielding, with subsequent states of damage progressing through concrete cracking, spalling, crack widening, reinforcement buckling, and concrete cover crushing. Column collapse occurs with the crushing of the concrete core at a column drift of 5%. FPS and LRB isolators are designed to accommodate certain displacements, but exceeding these limits can lead to failure as a second damage index. For bridges isolated with FPS and LRB bearings, the isolators are considered the most fragile structural components (Gkatzogias et al., 2022; Mahboubi et al. 2019). FPS and LRB isolators are designed to accommodate certain displacements, but exceeding these limits can lead to failure.

9.2. Development of Fragility Curves

The fragility analysis results for FPS-isolated bridges across all skew angles are presented in a single diagram, comparing five skew configurations. Each damage state is represented by a distinct fragility curve. The results indicate that the probability of damage systematically increases with higher skew angles. The fragility analysis across four damage states revealed a clear trend in bridge vulnerability with varying skew angles. Bridges with a 60° skew consistently exhibited the highest probability of failure when isolated with friction pendulum systems, particularly in the moderate-to-collapse damage range. In the slight damage state, this elevated vulnerability was noticeable up to 0.5 g PGA, with only a minor increase in failure probability beyond this level. For moderate and collapse states, the 60° skew bridge displayed failure probabilities approximately 10% higher than bridges with smaller skew angles, primarily due to torsional effects induced by deck inertia, which exacerbate deck-to-abutment collisions and contribute to more severe failure modes. The extensive damage state showed a similar pattern, though with notable variations among skew angles; for instance, at 1 g PGA, the 30° skew bridge exhibited a 7% higher failure probability than the 45° configuration. Overall, these results indicate a pronounced increase in failure probability for the 60° skew bridge across all damage states. In contrast, the 45° skew bridge consistently demonstrated more favorable seismic performance. This improved behavior is attributed to a more uniform distribution of seismic forces, which mitigates extreme torsional moments and reduces deck-to-abutment pounding. The 45° configuration facilitates more effective energy dissipation and a balanced dynamic response, allowing the bridge to better accommodate seismic demands across its structural components. Figure 8 illustrates the failure probabilities of bridges isolated with Lead Rubber Bearing (LRB) isolators. Across the slight, moderate, and extensive damage

states, the failure probabilities are largely comparable. However, a clear trend emerges in which higher skew angles correspond to increased failure likelihood. In the collapse damage state, the 60° skew bridge exhibits a failure probability exceeding 10% relative to lower skew angles, mirroring the behavior observed for FPS-isolated bridges. Consistently, the 45° skew bridge demonstrates the most favorable seismic performance. This superior behavior is attributed to a more uniform distribution of seismic forces, which reduces torsional effects and localized damage, allowing the structural system to dissipate energy effectively and mitigate critical failure modes. Consequently, the 45° configuration consistently exhibits lower probabilities of failure across all damage states.

Figure 8. Comparison of fragility curves of FPS models in four damage states in all skew angles (a) Slight, (b) Moderate, (c) Extensive, (d) Collapse

Figure 9 presents a comparison of the seismic performance of a zero-skew bridge using Incremental Dynamic Analysis, with fragility curves generated for four damage states. In the slight damage state, the performance of bridges isolated with both isolator types was nearly identical. At higher damage states, moderate, extensive, and collapse, the bridge with Lead Rubber Bearings (LRB) exhibited approximately 5% higher failure probabilities than the

bridge with Friction Pendulum Systems (FPS). This difference is attributed to the lower initial stiffness and damping capacity of LRBs at equivalent maximum design displacements, which reduces their effectiveness in mitigating seismic demands.
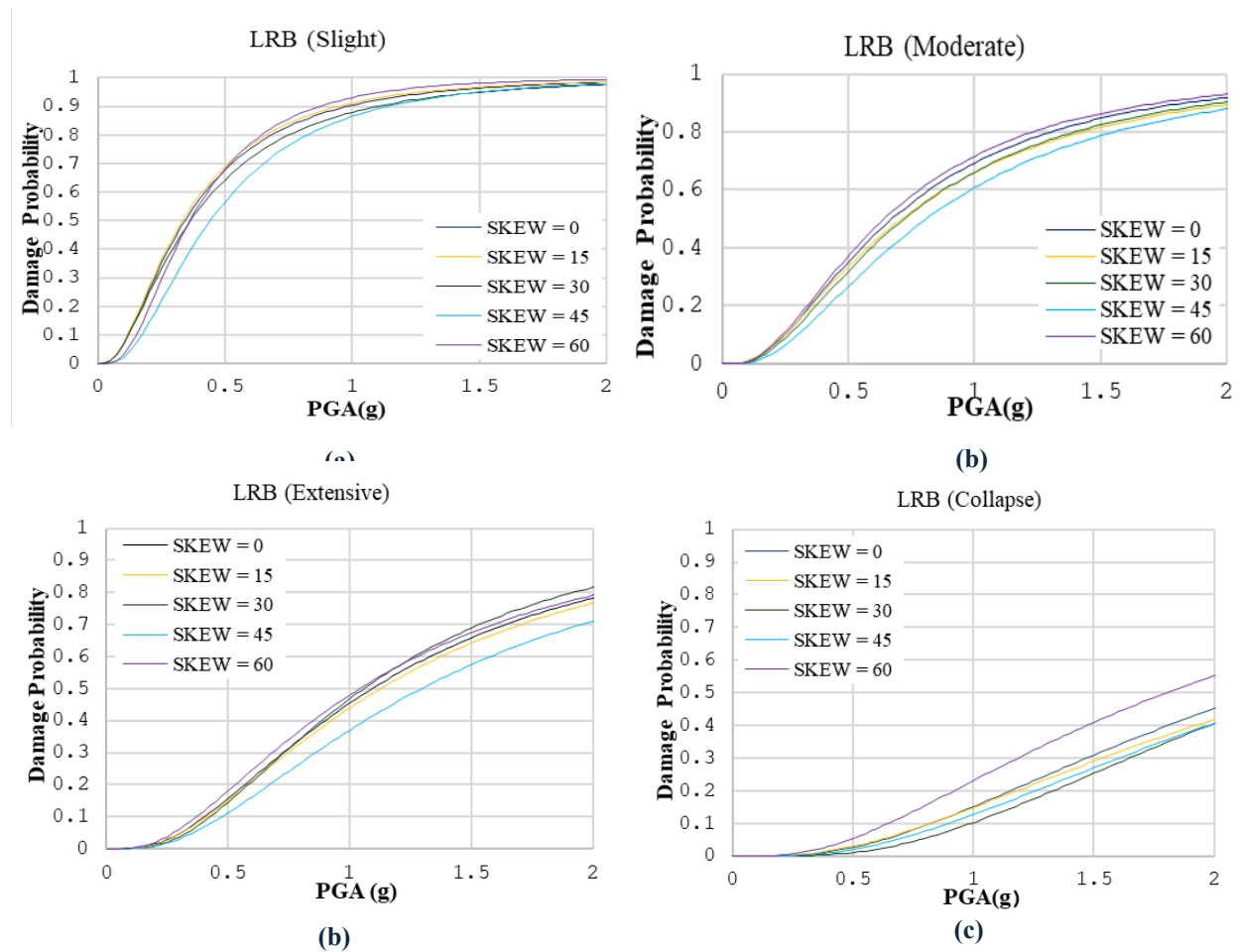

Figure 9. Comparison of fragility curves of FPS models in four damage states in all skew angles (a) Slight, (b) Moderate, (c) Extensive, (d) Collapse

Figure 10 presents a comparative analysis of failure probabilities for a 15° skew bridge isolated with Friction Pendulum System (FPS) and Lead Rubber Bearing (LRB) isolators. At the slight damage level, the failure probability of the LRB-isolated bridge is approximately 4% higher than that of the FPS bridge at 0.5g PGA. This difference decreases to 2% at the moderate damage level, with the FPS system consistently exhibiting lower failure probabilities. At the extensive damage level, the disparity increases, with LRB showing a failure probability roughly 7% higher than FPS at 1.5 g PGA. For the collapse damage state, failure probabilities are comparable between the two isolator types. Overall, as observed for non-skew bridges, FPS

provides superior seismic performance, primarily due to its higher initial stiffness and damping, which more effectively dissipate energy through friction.
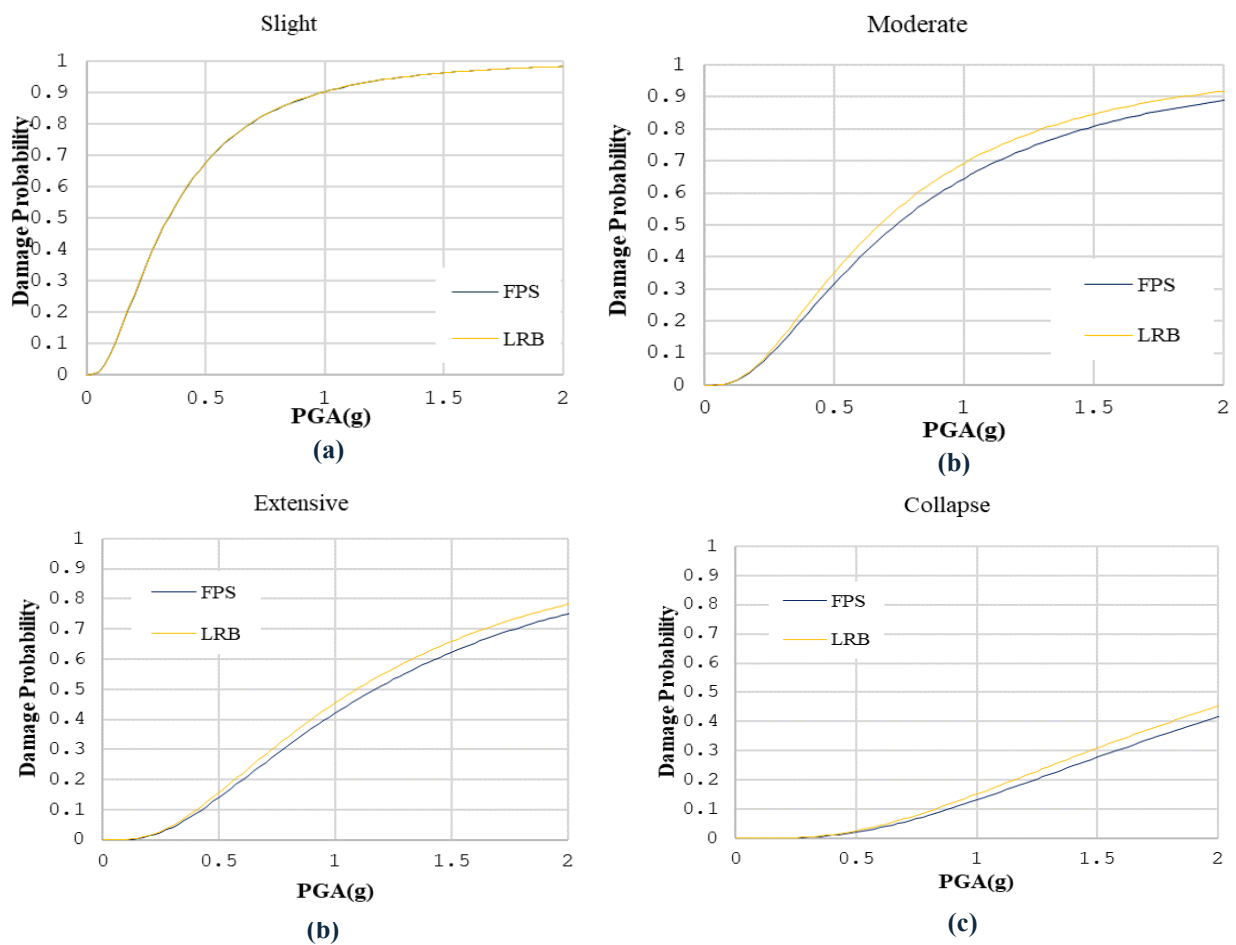

Figure 10. Comparison between FPS and LRB in skew angles of 0 in all damage indices (a) Slight, (b) Moderate, (c) Extensive, (d) Collapse.
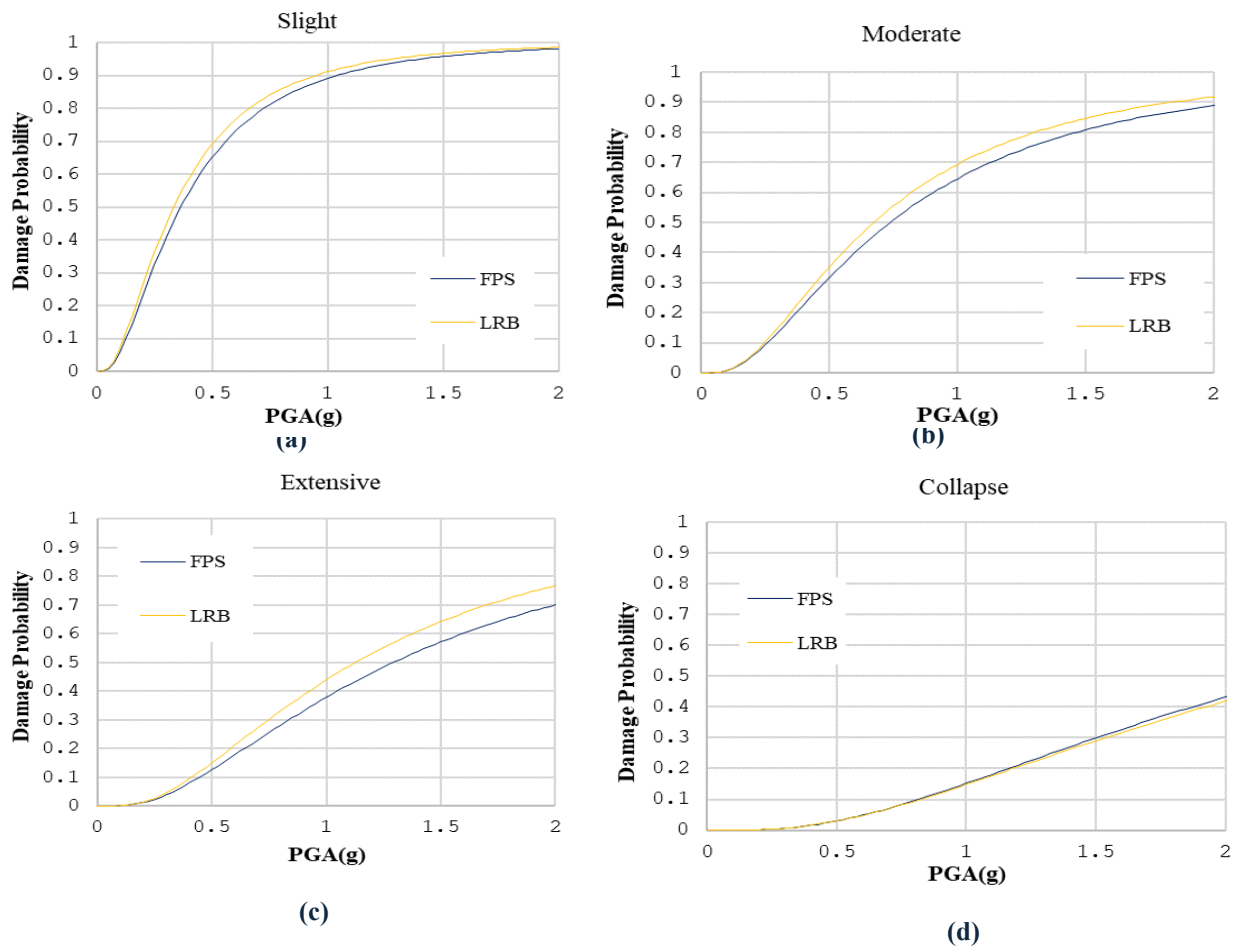
Figure 11. Comparison between FPS and LRB in skew angles of 15 in all damage indices (a) Slight, (b) Moderate, (c) Extensive, (d) Collapse

Figure 12 illustrates the bridge performance for both isolator types at a 30° skew angle. At the slight damage level, failure probabilities are nearly identical. At the moderate damage level, the LRB- isolated bridge exhibits a 1% higher failure probability. This disparity becomes more pronounced at the extensive damage level, with LRB showing approximately 8% higher failure probability at 1.5 g PGA. For the collapse damage state, the difference between the two isolator types diminishes, and the bridge performance is similar for both FPS and LRB systems.
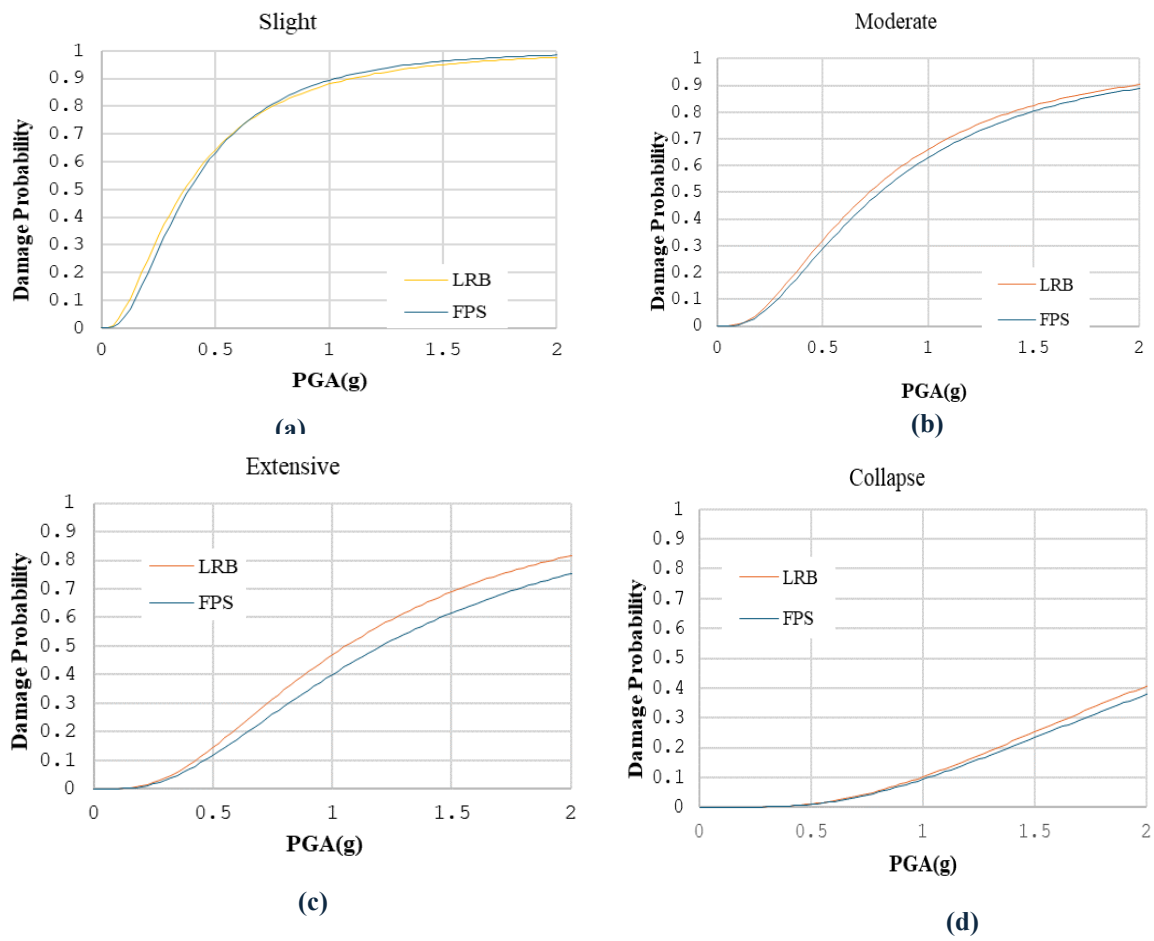
Figure 12. Comparison between FPS and LRB in skew angles of 30 in all damage indices (a) Slight, (b) Moderate, (c) Extensive, (d) Collapse.
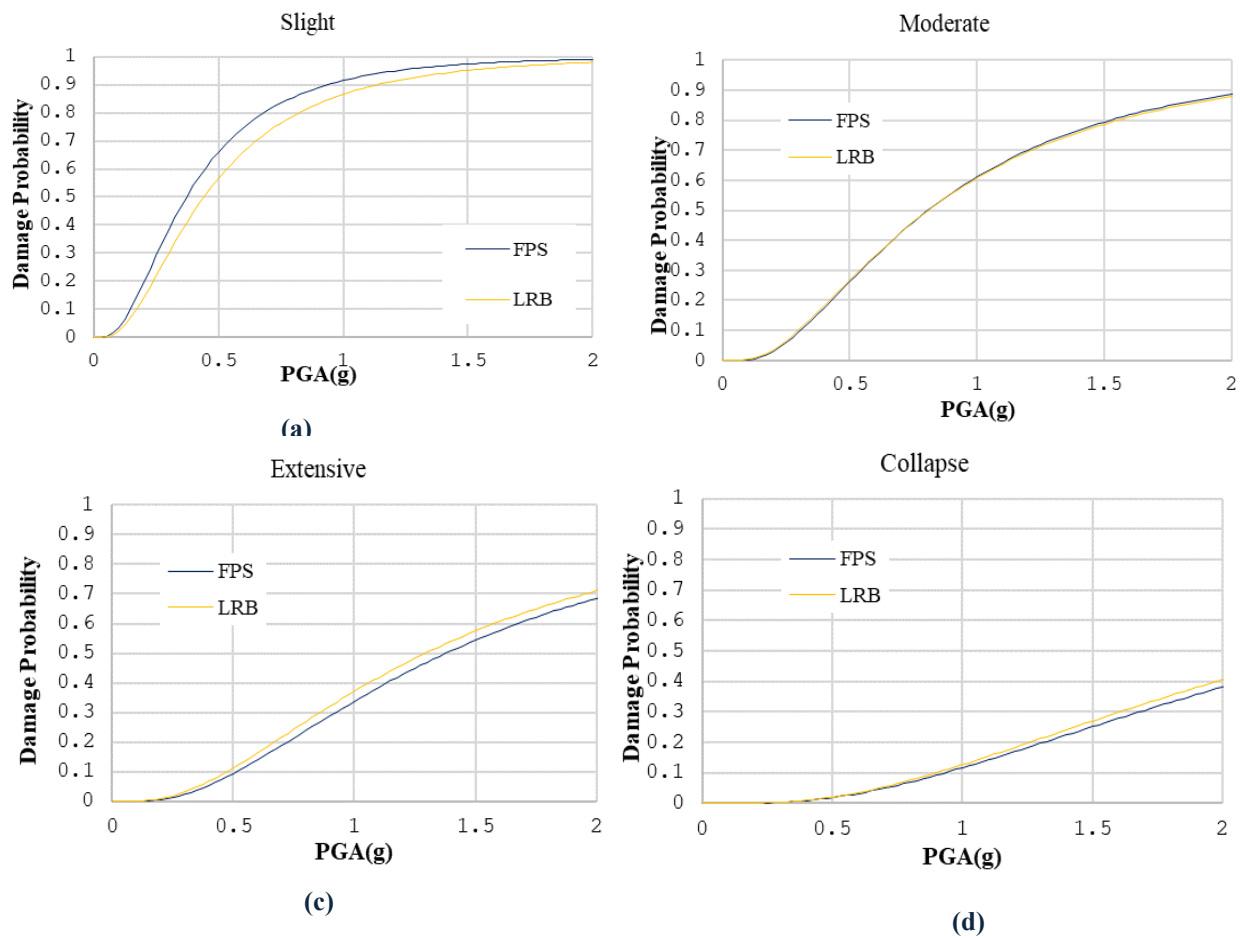
Figure 13. Comparison between FPS and LRB in skew angles of 45 in all damage indices (a) Slight, (b) Moderate, (c) Extensive, (d) Collapse.

As the skew angle increases, the fundamental periods of the bridge modes also increase, influenced by torsional effects and deck-to-deck pounding induced by deck torsion. Figure 16 shows that at a 45° skew angle, bridges with Friction Pendulum Systems (FPS) exhibit a slightly higher probability of slight-damage failure compared to Lead Rubber Bearings (LRB), primarily due to the distribution of inertial forces that amplifies torsional effects and deck pounding. The relatively lower initial stiffness of LRBs reduces their vulnerability at this skew angle. For moderate to severe damage states, the effect of the 45° skew is minor and comparable to other skew configurations, reflecting the FPS isolator's higher initial stiffness under small horizontal forces. However, at higher damage levels, the trend reverses: at the extensive damage level, LRB exhibits a higher failure probability—for example, approximately 4% higher at 1 g PGA. At the collapse state, the difference diminishes, with LRB showing only a 1% higher failure probability.
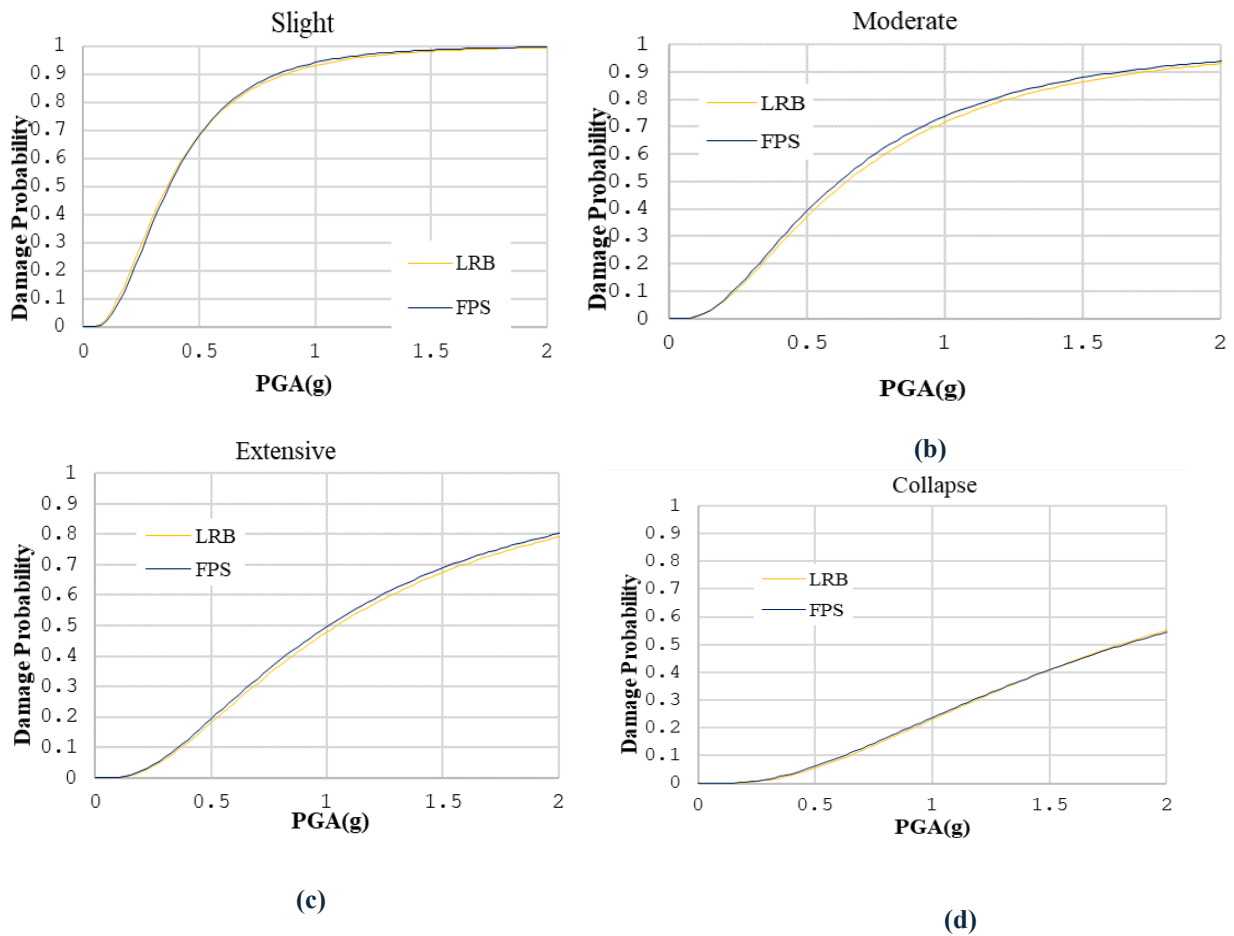
Figure 14. Comparison between FPS and LRB in skew angle of 60 in all damage indices (a) Slight, (b) Moderate, (c) Extensive, (d) Collapse.

The trends observed for the 45° skew bridge are similarly reflected in the 60° skew configuration, as shown in Figure 15. At this high skew angle, torsional effects dominate, resulting in comparable performance between FPS and LRB isolators at the slight damage level. At moderate and extensive damage states, the LRB exhibits slightly lower failure probabilities, approximately 1% less than FPS. This trend persists at the collapse damage level. Across all damage states and skew angles, bridges with FPS isolators generally show slightly higher failure probabilities than those with LRB, with differences averaging around 2% for most angles and damage levels. Interestingly, despite the higher stiffness and damping of FPS, their use can produce a minor counterintuitive effect on failure probability under certain torsion-dominated configurations, similar to the inverse effect observed for the 45° skew. Nevertheless, this effect is small and can be considered negligible in practical assessments. Figure 18 presents a comparative analysis of bridge failure probabilities based on the maximum isolator displacement criterion, evaluating two isolator types across multiple skew angles. The results indicate that bridges isolated with Lead Rubber Bearings (LRB) consistently exhibit higher failure probabilities than those with Friction Pendulum Systems (FPS). At a PGA of

0.6 g, the differences in failure probability across the five skew angles were 11%, 13%, 14%, 22%, and 12%, respectively. FPS outperformed LRB across all configurations, also demonstrating lower failure probabilities based on the column drift damage index.
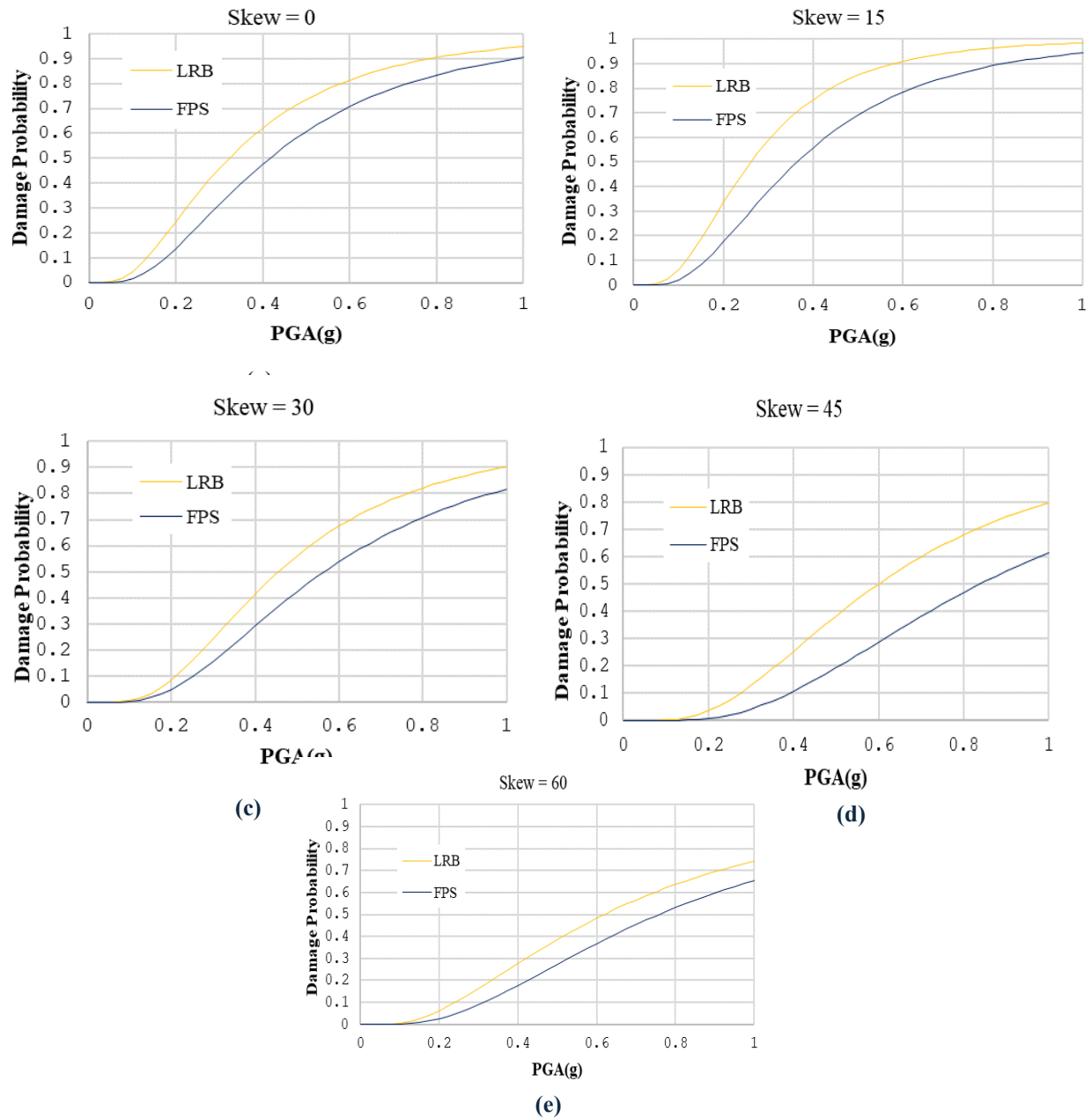

Figure 15. Comparisons of probability of failure with FPS and LRB isolator and fragility analysis

10. Conclusions

This study investigated the seismic vulnerability of RC bridges isolated with Friction Pendulum Systems (FPS) and Lead Rubber Bearings (LRB), with particular emphasis on the effect of skew angle through probabilistic analysis. The findings reveal a complex interaction between

isolator type, bridge geometry, and failure probability, with several important implications for seismic design:

1. Bridges with a 60° skew angle consistently exhibited the highest probability of failure across all damage states, regardless of isolator type. This was especially pronounced in the extensive and collapse damage levels, highlighting that extreme skew angles introduce significant torsional effects and design challenges that substantially elevate seismic risk. These effects become particularly critical under the pulse-type motions typical of near-fault earthquakes.

2. By comparison, bridges with a 45° skew angle demonstrated noticeably lower failure probabilities for both isolator types. This improved performance is attributed to a more uniform decomposition of torsional effects induced by seismic inertia. Being near the midpoint of the 0–90° skew range, this angle allows for a more balanced distribution of seismic forces, reducing the likelihood of critical failure compared to other configurations.

3. Comparative analysis showed that FPS generally provides superior performance, resulting in lower failure probabilities based on column drift criteria. For most skew angles, particularly up to 30°, the performance advantage of FPS over LRB was approximately 5%, with the difference increasing to about 10% across larger skew angles. The enhanced performance of FPS is due to its higher initial stiffness, greater damping, and frictional energy dissipation, which more effectively control seismic demands on the substructure.

4. Across damage states, the interaction between skew angle and isolator type is notable. At slight damage levels, differences between isolators are minor, while at moderate to extensive damage levels, FPS consistently outperforms LRB. For collapse-level damage, the differences decrease slightly but FPS generally maintains lower failure probabilities.

5. Overall, these results emphasize that both isolator type and bridge geometry critically influence seismic performance. The study highlights the particular vulnerability of bridges with a 60° skew angle and confirms that FPS isolators can provide superior seismic protection across all skew configurations. These insights are essential for designers seeking to optimize the seismic resilience of skewed bridges under near-fault excitations.

11. References

Abdel-Mohti, Ahmed, and Gokhan Pekcan. 2013a. "Assessment of Seismic Performance of Skew Reinforced Concrete Box Girder Bridges." *International Journal of Advanced Structural Engineering* 5 (1): 1. https://doi.org/10.1186/2008-6695-5-1.

Aldea, Sofía, Ramiro Bazáez, Pablo Heresi, and Rodrigo Astroza. 2024. "Effect of Bidirectional Hysteretic Dampers on the Seismic Performance of Skewed Multi-Span Highway Bridges." *Buildings*. https://doi.org/10.3390/buildings14061778.

Argyroudis, Sotirios A, Stergios A Mitoulis, Lorenzo Hofer, Mariano Angelo Zanini, Enrico Tubaldi, and Dan M Frangopol. 2020. "Resilience Assessment Framework for Critical Infrastructure in a Multi-Hazard Environment: Case Study on Transport Assets." *Science of The Total Environment* 714:136854. https://doi.org/https://doi.org/10.1016/j.scitotenv.2020.136854.

Ateş, Serenay, and Özgür Avşar. 2024. "Seismic Performance of Skewed Bridges with Uniform and Non-Uniform Scour." *Soil Dynamics and Earthquake Engineering* 187:108976. https://doi.org/https://doi.org/10.1016/j.soildyn.2024.108976.

Bouassida, Y, E Bouchon, P Crespo, P Croce, L Davaine, S Denton, M Feldmann, et al. 2012. *Bridge Design to Eurocodes*. *JRC, European Commission*. Vol. 1. https://doi.org/10.2788/82360.

Bouassida, Yorsa, Emmanuel Bouchon, Pilar Crespo, Pietro Croce, Laurence Davaine, Steve Denton, Markus Feldmann, Roger Frank, Gerhard Hanswille, and Wolfang Hensen. 2012. "Bridge Design to Eurocodes-Worked Examples." *Work."Bridge Des. to Eurocodes," Vienna*, 4–6.

Chen, Jingyi, Qiang Han, Xiao Liang, and Xiuli Du. 2017. "Effect of Pounding on Nonlinear Seismic Response of Skewed Highway Bridges." *Soil Dynamics and Earthquake Engineering* 103:151–65. https://doi.org/https://doi.org/10.1016/j.soildyn.2017.09.008.

Chen, Peng, Yuhang Lu, Bin Wang, Peng Zhuang, and Kaoshan Dai. 2025. "Enhancing Seismic Resilience in Base-Isolated Structures: A Performance-Based Comparison of HDRB and LRB Isolation Systems." *Engineering Structures* 342:120945.

Coletti, Domenic, Brandon Chavel, and Walter J Gatti. 2011. "Challenges of Skew in Bridges with Steel Girders." *Transportation Research Record* 2251 (1): 47–56. https://doi.org/10.3141/2251-05.

Constantinou, Michael C, Panos Tsopelas, Amarnath Kasalanati, Eric D Wolff, and Ketter Hall. 1999. "Property Modification Factors for Seismic Isolation Bearings By."

Dicleli, Murat. 2002. "Seismic Design of Lifeline Bridge Using Hybrid Seismic Isolation." *Journal of Bridge Engineering* 7 (2): 94–103. https://doi.org/10.1061/(asce)1084-0702(2002)7:2(94).

Dong, You, and Dan M Frangopol. 2015. "Risk and Resilience Assessment of Bridges under Mainshock and Aftershocks Incorporating Uncertainties." *Engineering Structures* 83:198–208. https://doi.org/https://doi.org/10.1016/j.engstruct.2014.10.050.

Dutta, Anindya, and John B Mander. 1998. "Capacity Design and Fatigue Analysis of Confined Concrete Columns." State University of New York at Buffalo. Department of Civil, Structural ….

FHWA-NHI-15-004. 2014. "LRFD Seismic Analysis and Design of Bridges - Reference Manual," no. FHWA-NHI-15-004, 608.

Gkatzogias, Konstantinos I, and Andreas J Kappos. 2022. "Deformation-based Design of Seismically Isolated Bridges." *Earthquake Engineering & Structural Dynamics* 51 (14): 3243–71.

Jara, J M, B A Olmos, M Jara, and W M Conejo. 2016. "RC Jacketing Parameters to Retrofit Highway Bridges." *Bulletin of Earthquake Engineering* 14 (10): 2859–80. https://doi.org/10.1007/s10518-016-9914-7.

Koks, Elco E, Julie Rozenberg, Conrad Zorn, Mersedeh Tariverdi, Michalis Vousdoukas, Stuart Alexander Fraser, J W Hall, and Stephane Hallegatte. 2019. "A Global Multi-Hazard Risk Analysis of Road and Railway Infrastructure Assets." *Nature Communications* 10 (1): 2677.

Lee, Tae-Hyung, and Duy-Duan Nguyen. 2018. "Seismic Vulnerability Assessment of a Continuous Steel Box Girder Bridge Considering Influence of LRB Properties." *Sādhanā* 43 (1): 14. https://doi.org/10.1007/s12046-017-0774-x.

Mahboubi, S., and. Shiravand. M.R. 2019. "Proposed Input Energy-Based Damage Index for RC Bridge Piers." *Journal of Bridge Engineering* 24 (1): 4018103. https://doi.org/10.1061/(asce)be.1943-5592.0001326.

Mander, John B. 1999. "Fragility Curve Development for Assessing the Seismic Vulnerability of Highway Bridges." *Research Progress And* 89.

Meng, Jun Yi, and Eric M Lui. 2000. "Seismic Analysis and Assessment of a Skew Highway Bridge." *Engineering Structures* 22 (11): 1433–52.

Naeim, Farzad, and James M Kelly. 1999. *Design of Seismic Isolated Structures: From Theory to Practice*. John Wiley & Sons.

Nielson, Bryant G. 2005. *Analytical Fragility Curves for Highway Bridges in Moderate Seismic Zones*. Georgia Institute of Technology.

Nielson, Bryant G, and Reginald DesRoches. 2007. "Analytical Seismic Fragility Curves for Typical Bridges in the Central and Southeastern United States." *Earthquake Spectra* 23 (3): 615–33.

Noori, H R, M M Memarpour, M Yakhchalian, and S Soltanieh. 2019. "Effects of Ground Motion Directionality on Seismic Behavior of Skewed Bridges Considering SSI." *Soil Dynamics and Earthquake Engineering* 127:105820. https://doi.org/https://doi.org/10.1016/j.soildyn.2019.105820.

Ozer, Esra, and Mehmet Inel. 2025. "The Effect of Single and Combined Use of Base Isolator and Fluid Viscous Damper on Seismic Performance in a Conventional RC Building with Torsional Irregularity." *Journal of Building Engineering* 101:111898. https://doi.org/https://doi.org/10.1016/j.jobe.2025.111898.

Padgett, Jamie E, and Reginald DesRoches. 2008. "Methodology for the Development of Analytical Fragility Curves for Retrofitted Bridges." *Earthquake Engineering & Structural Dynamics* 37 (8): 1157–74.

Park, R, and T Paulay. 1975. "Ductile Reinforced Concrete Frames: Some Comments on the Special Provisions for Seismic Design of ACI 318-71 and on Capacity Design." *Bulletin of the New Zealand Society for Earthquake Engineering* 8 (1): 70–90.

Pranesh, M., and Ravi Sinha. 2000. "VFPI: An Isolation Device for Aseismic Design." *Earthquake Engineering and Structural Dynamics* 29 (5): 603–27. https://doi.org/10.1002/(SICI)1096-9845(200005)29:5<603::AID-EQE927>3.0.CO;2-W.

Priestley, M J Nigel, Frieder Seible, and Gian Michele Calvi. 1996. *Seismic Design and Retrofit of Bridges*. John Wiley & Sons.

Ramanathan, Karthik, Reginald DesRoches, and Jamie E Padgett. 2012. "A Comparison of Pre- and Post-Seismic

Design Considerations in Moderate Seismic Zones through the Fragility Assessment of Multispan Bridge Classes." *Engineering Structures* 45:559–73. https://doi.org/https://doi.org/10.1016/j.engstruct.2012.07.004.

Robinson, William H. 2011. "Lead-Rubber Hysteretic Bearings Suitable for Protecting Structures during Earthquakes." *Seismic Isolation and Protective Systems* 2 (1): 5–19. https://doi.org/10.2140/siaps.2011.2.5.

Shid, Golshid, Shiravand, M.R. and Mahboubi. S. 2025. "Direction Effect of Vertical Ground Motion on Seismic Damages of Friction-Based Isolated RC Piers." *Advances in Bridge Engineering* 6 (1): 9. https://doi.org/10.1186/s43251-024-00154-0.

Smith, Alec W, Sotirios A Argyroudis, Mike G Winter, and Stergios A Mitoulis. 2021. "Economic Impact of Bridge Functionality Loss from a Resilience Perspective: Queensferry Crossing, UK." In *Proceedings of the Institution of Civil Engineers-Bridge Engineering*, 174:254–64. Thomas Telford Ltd.

Son, Jin-Su, Won Jong Chin, Chang Beck Cho, and Jin-Young Lee. 2025. "FHWA." *Journal of Disaster Science and Management* 1 (1): 9.

Yin, Weitao, Kehai Wang, and Weizuo Guo. 2023. "Determination of Reasonable Parameters for Skew Bridge under Different Skew Angles." *Journal of Vibroengineering* 25 (4): 729–44. https://doi.org/10.21595/jve.2022.22907.

Zayas, Victor A., Stanley S. Low, and Stephen A. Mahin. 1990. "A Simple Pendulum Technique for Achieving Seismic Isolation." *Earthquake Spectra*. https://doi.org/10.1193/1.1585573.